Nuclear Materials and Energy 26 (2021) 100904

Contents lists available at ScienceDirect

Nuclear Materials and Energy

journal homepage: www.elsevier.com/locate/nme

A sensitivity analysis of numerical predictions for beryllium erosion and migration in ITER

J. Romazanov [a,*], S. Brezinsek [a], R.A. Pitts [b], A. Kirschner [a], A. Eksaeva [a], D. Borodin [a], E. Veshchev [b], V.S. Neverov [c], A.B. Kukushkin [c], A.G. Alekseev [c], Ch. Linsmeier [a]

[a] Forschungszentrum Jülich GmbH, Institut für Energie- und Klimaforschung – Plasmaphysik, Partner of the Trilateral Euregio Cluster (TEC), 52425 Jülich, Germany

[b] ITER Organization, Route de Vinon-sur-Verdon, CS 90 046, 13067, St. Paul Lez Durance Cedex, France

[c] National Research Centre 'Kurchatov Institute', Moscow 123182, Russia

ARTICLE INFO

Keywords:
Beryllium
Erosion
Migration
ERO2.0
ITER

ABSTRACT

The present study addresses the uncertainties that affect the recently performed predictions of beryllium (Be) erosion and migration in ITER using the Monte-Carlo code ERO2.0. The focus of the study is a D–T baseline discharge with fusion power gain $Q = 10$, scrape-off layer (SOL) input power $P_{SOL} = 100$ MW, toroidal plasma current $I_p = 15$ MA, and central toroidal field $B_t = 5.3$ T. The parameter studies used to investigate uncertainties include variations of the radial extrapolation of plasma parameters in the far-SOL (scan A), the assumptions on impact angle distributions (scan B) and the anomalous transport of eroded Be (scan C). Variations by factors ~ 3, ~ 18 and ~ 2 for scans A, B and C, respectively, are found.

1. Introduction

Steady-state erosion of the ITER main chamber first wall (FW) beryllium (Be) armour is expected to affect several processes important for the reactor duty cycle. Among these are armour degradation and lifetime, dust formation, and release of Be impurities potentially leading to enhanced sputtering of the W divertor [1] and tritium retention due to co-deposition [2]. Reliable numerical estimations of the Be erosion and migration are necessary to quantify these effects, but also to support the development of ITER diagnostics, designed for monitoring the Be primary source, by providing synthetic signals.

The Monte-Carlo code ERO was used in the past to investigate local Be erosion of selected FW panels [3], followed by global modelling including all FW panels using the upgraded code ERO2.0 [4,5]. The code simulates the steady-state Be erosion flux resulting from ion and charge-exchange (CX) neutral bombardment of the entire ITER FW, taking into account the subsequent kinetic transport of eroded Be impurities. The latter are represented by so-called test particles, which are used in a Monte-Carlo formalism to solve the Fokker–Planck equation in the trace impurity approximation [6]. The three-dimensional (3D) shaping of the FW panels is taken into account, which is important due to magnetic shadowing effects affecting the flux distribution and the strong dependence of sputtering yields on the particle impact angle.

The present work addresses the sensitivity of the ERO2.0 predictions regarding (1) the extrapolation of plasma parameters near the FW panel surfaces, (2) the assumptions on particle impact angle distributions, and (3) the anomalous transport of Be ions in the plasma. The main results of the modelling studies are summarized in Table 1.

2. Parameter studies

2.1. Reference modelling assumptions

All simulations in this study are based on the baseline H-mode D–T burning plasma scenario with toroidal plasma current $I_p = 15$ MA, central toroidal field $B_t = 5.3$ T, fusion power gain $Q = 10$, and input power $P_{SOL} = 100$ MW into the scrape-off layer (SOL) [7] ("reference case"). This scenario is labelled "case #1" in the wider study reported in [5], where other plasma scenarios are also considered.

SOLPS-4.3 coupled to OEDGE [8] simulations provide the input plasma background (PBG) to ERO2.0, i.e. the two-dimensional (2D) distribution of plasma parameters in the boundary region. OEDGE extends the grid to the wall using a combination of onion skin modelling (OSM) and the kinetic neutral transport code EIRENE [9]. In addition, OEDGE considers the so-called ITER Heat and Nuclear Load Specifications (HNLS) [10] as a constraint for the far-SOL plasma. Importantly, the HNLS implies flat temperature profiles in the SOL with $T_e \approx 10$ eV and $T_i \approx 20$ eV [4,5,8]. The OEDGE extended grid and the underlying

* Correspondence to: JARA-HPC, Jülich Supercomputing Centre, Forschungszentrum Jülich GmbH, Jülich 52425, Germany.
E-mail address: j.romazanov@fz-juelich.de (J. Romazanov).

https://doi.org/10.1016/j.nme.2021.100904
Received 21 September 2020; Received in revised form 18 December 2020; Accepted 4 January 2021
Available online 14 January 2021

Table 1
Summary of the surface-integrated Be erosion and deposition results of the parametric studies in comparison with the reference case.

	–	Parameter scan A		Parameter scan B					Parameter scan C	
Description:	Reference case	$\lambda = 0.1$ cm	$\lambda = 1$ cm	$\theta = 0°$	$\theta = 60°$	$\theta = 75°$	$\theta = 80°$	$\theta = 85°$	$D_\perp = 0.3\,m^2/s$	$D_\perp = 10\,m^2/s$
FW gross erosion [Be/s]	$1.53\cdot10^{23}$	$5.50\cdot10^{22}$	$7.57\cdot10^{22}$	$1.28\cdot10^{22}$	$1.07\cdot10^{23}$	$2.08\cdot10^{23}$	$2.35\cdot10^{23}$	$2.34\cdot10^{23}$	$1.96\cdot10^{23}$	$9.74\cdot10^{22}$
… by D^+ impact [%]	20.7	12.7	15.4	27.6	27.8	27.4	27.4	27.4	16.1	32.5
… by D^0 impact [%]	23.1	64.5	46.8	15.9	15.7	15.8	15.9	15.8	18.1	36.4
… by Be^Z impact [%]	56.2	22.9	37.8	56.5	56.5	56.8	56.7	56.7	65.8	31.1
FW net erosion [Be/s]	$1.50\cdot10^{22}$	$9.37\cdot10^{21}$	$1.03\cdot10^{22}$	$1.21\cdot10^{21}$	$1.01\cdot10^{22}$	$1.96\cdot10^{22}$	$2.22\cdot10^{22}$	$2.20\cdot10^{22}$	$2.01\cdot10^{22}$	$6.89\cdot10^{21}$
FW gross deposition [Be/s]	$1.35\cdot10^{23}$	$4.49\cdot10^{22}$	$6.39\cdot10^{22}$	$1.13\cdot10^{22}$	$9.44\cdot10^{22}$	$1.83\cdot10^{23}$	$2.07\cdot10^{23}$	$2.06\cdot10^{23}$	$1.73\cdot10^{23}$	$8.82\cdot10^{22}$
FW gross deposition [%]	90.0	82.7	86.1	90.3	90.3	90.4	90.3	90.4	89.6	92.8
Divertor gross deposition [Be/s]	$1.47\cdot10^{22}$	$9.08\cdot10^{21}$	$9.99\cdot10^{21}$	$1.19\cdot10^{21}$	$9.91\cdot10^{21}$	$1.92\cdot10^{22}$	$2.18\cdot10^{22}$	$2.16\cdot10^{22}$	$1.99\cdot10^{22}$	$5.80\cdot10^{21}$
Divertor gross deposition [%]	9.8	16.7	13.5	9.5	9.5	9.5	9.5	9.5	10.3	6.1
Gaps gross deposition [Be/s]	$2.95\cdot10^{20}$	$2.93\cdot10^{20}$	$2.87\cdot10^{20}$	$2.27\cdot10^{19}$	$1.86\cdot10^{20}$	$3.60\cdot10^{20}$	$4.18\cdot10^{20}$	$4.25\cdot10^{20}$	$1.85\cdot10^{20}$	$1.09\cdot10^{21}$
Gaps gross deposition [%]	0.2	0.5	0.4	0.2	0.2	0.2	0.2	0.2	0.1	1.1

SOLPS-4.3 solution regions are shown in Fig. 1(a), which also shows the magnetic configuration and the locations of the 18 FW panels in the ITER poloidal cross-section. Note that both SOLPS-4.3 and OEDGE are 2D codes, so that the resulting 2D PBG cannot account for the toroidal FW shaping and is thus assumed to extend only to the innermost radial ridges of FW panels in the poloidal cross-section. This necessitates the extrapolation of plasma profiles in the radial outward direction, as discussed in detail in the next section. In addition, numerical tracing of magnetic field lines is used to define plasma-wetted and shadowed areas (the latter are excluded from erosion by ions) on the 3D surface, as shown in Fig. 1(b). The shadowing model is described in detail in [4].

The simulations with the massively-parallelized ERO2.0 code were performed on the JURECA supercomputer [12]. The requirement for supercomputing resources comes from the large number of Be test particles (10^6 for the calculations reported here) that are necessary in production runs to achieve sufficiently reproducible results with acceptable Monte-Carlo noise. As a simplification, the D–T plasma is described as a pure D plasma (as is the case, in fact, for the SOLPS-4.3 PBG simulations). Furthermore, Be is considered in ERO2.0 to be the only impurity, though the PBG includes neon seeding for power dissipation in the divertor, which can be neglected for the current study focussing on the main chamber.

The Be sputtering yields used to calculate the Be erosion are discussed in more detail in [5]. Note that chemically assisted physical sputtering with release of BeD molecules [13] is neglected here for simplicity, so that all erosion is assumed to be in the form of Be atoms.

In the following, the individual parameter scans will be presented. Note that during each scan, all other parameters are kept as in the reference case (as explained in more detail below), namely: (1) constant extrapolation of radial temperature profiles; (2) non-constant impact angles for deuterium ions and neutrals; (3) diffusion coefficient $D_\perp = 1.0\,m^2/s$ for Be ions.

To compare the simulations, we focus on the figure of total Be gross erosion, which is obtained by integrating over the full main chamber surface area (1.53×10^{23} Be/s in the reference case). A deeper interpretation of the results in view of reactor operation (e.g. in terms of tritium retention, dust production or wall lifetime resulting from peak net erosion) is beyond the scope of this work.

2.2. Parameter scan A: Influence of far-SOL plasma conditions

Some modifications of the OEDGE data are required due to the 3D shaping of the FW panels considered in the ERO2.0 modelling. Despite the extended grid in the PBG, the shaping leads to a small gap Δr_{gap} between the outer OEDGE grid and the FW surface cells. The gap size is mostly about 0–3 cm in the plasma-wetted areas, as shown in Fig. 1(b). To be consistent with the flat plasma temperature profiles in OEDGE prescribed by the (conservative) ITER HNLS, the reference approach in ERO2.0 is to extend the radial temperature profiles in the gap region using constant extrapolation, as shown in the outer mid-plane (OMP) profiles in Fig. 2 (the same extrapolation approach is used for the plasma density and flow velocity profiles).

To investigate the effect of a less conservative assumption about temperature profiles, an exponential radial decay was applied to those, resulting in lower ion impact energies and hence Be erosion. In the frame of "parameter scan A" described in this section, different decay lengths, $\lambda = 0.1$ cm, 1.0 cm and 10.0 cm, were considered for the extrapolation of T_e and T_i (assuming the same decay length for both) beyond the OEDGE grid boundary, as depicted in Fig. 2.

For simplicity, the density and flow velocity profiles were not changed during this scan. It should be noted that when reducing the temperature, the flux distribution of impinging D ions is affected via the reduced sound velocity; however, the total (surface-integrated) D ion flux was artificially kept constant during the scan to maintain particle balance with OEDGE and to simplify the interpretation.

The above values of λ are selected on the basis of typical experimental values from various plasma devices, which are scattered within the range of $\lambda \sim 0.1$–10 cm.[1] Furthermore, numerical estimates were performed using the connection lengths L calculated by ERO2.0 field line tracing, combined with either diffusive or convective models for $\lambda(L)$ and the associated perpendicular transport to the wall. The considered range of input parameters (e.g. $D = 0.1$–$10.0\,m^2/s$ for the diffusive model) again led to $\lambda \sim 0.1$–10 cm, so that the parametric approach chosen here seems reasonable.

[1] See Figures 21.1, 21.2, 21.3, 21.8, 21.9 and 23.2 in [14].

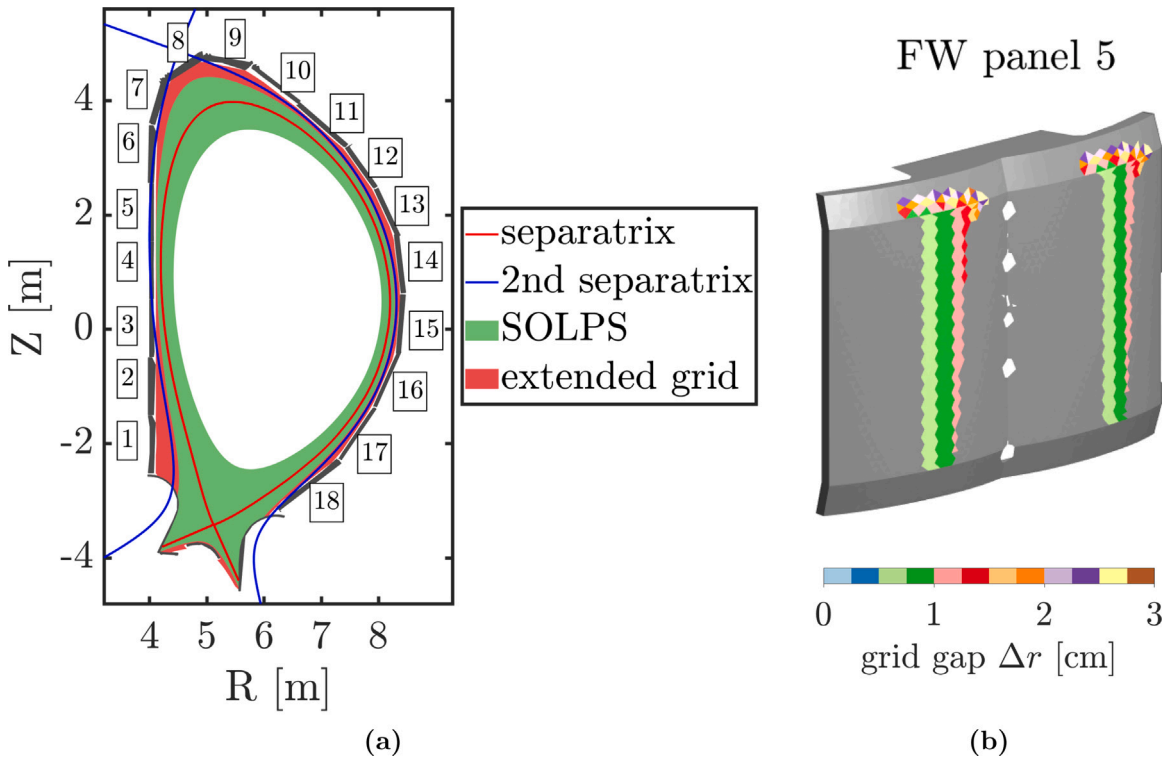

Fig. 1. (a) Poloidal view of the simulated ITER geometry. The black patches numbered 1–18 indicate the individual FW panels. The coloured regions indicate the SOLPS-4.3 grid and the "extended grid" of the OEDGE solution. (b) Zoomed in 3D view of panel 5, with a colour map indicating the distance of plasma-wetted surfaces from the OEDGE grid boundary. Grey areas are indicating magnetically shadowed areas, which are assumed to have zero erosion. The circular openings in the centre of the panel are remote handling access holes [11].

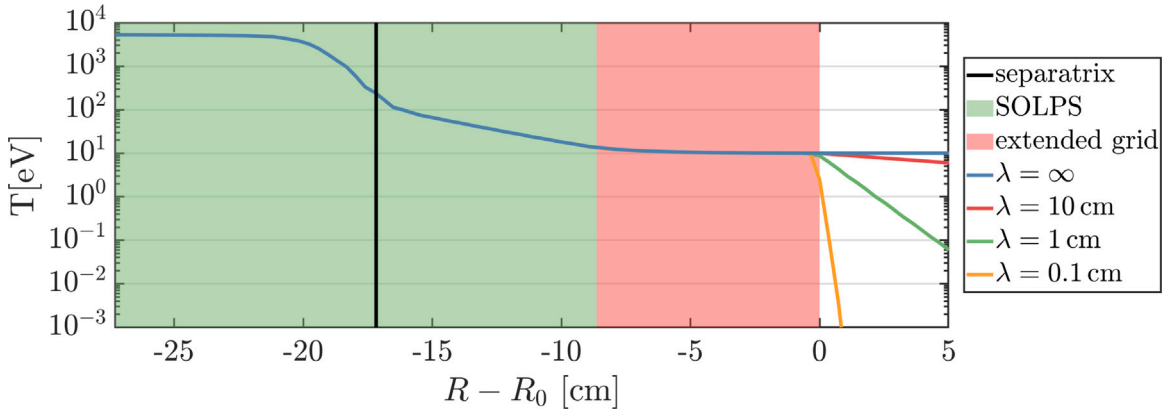

Fig. 2. Outer midplane (OMP) profiles of the electron temperature. R_0 is the OEDGE outer grid boundary at the OMP. The reference case with a constant extrapolation ($\lambda = \infty$) is compared to exponentially decaying profiles obtained with a finite λ.

Preliminary simulations have shown that there is no appreciable difference in the Be erosion pattern and magnitude between the λ = 10.0 cm and $\lambda = \infty$ cases. The former is therefore not further considered here in the following.

Fig. 3 shows the Be erosion rate integrated over the entire ITER FW. The contribution to the erosion by D^0 impact is by definition constant because ERO2.0 imports D^0 fluxes and energies directly from EIRENE (run as part of OEDGE), which are therefore not affected by the plasma parameter extrapolation. In contrast, the contribution by D^+ impact is decreased for smaller λ because the D^+ impact energy is proportional to T_e (determining the sheath potential) and T_i (determining the ion energy at the sheath entrance). Likewise, the contribution due to Be^{Z+} impact is decreased for smaller λ both because fewer Be particles are eroded in the first place, and due to a decrease in their impact energy by the lower sheath potential.

In the λ = 1 cm case, the total erosion is decreased by 50 % compared to the reference $\lambda = \infty$ case. For λ = 0.1 cm, the decrease is 65 %. With decreasing λ, the eroded areas are reducing in toroidal direction to a small poloidal stripe around the panel ridges (green areas in Fig. 1(b)). It is expected that further reduction below 0.1 cm would only lead to a gradual decrease in erosion (saturation effect), because some regions exist with a very small gap $\Delta r \ll 0.1$ cm or even with no gap, which are not subject to the extrapolation.

It should be noted that λ = 0.1 cm is already at the lower end of the experimental values found in literature and the numerical estimations using a diffusive or convective model. Values of (density or temperature) decay lengths $\lambda \sim$ 1 cm or higher seem more probable. Thus, the result of this scan in the far-SOL plasma parameter extrapolation may be summarized by noting that the conservative assumption of $\lambda = \infty$ likely leads to an overestimation of the Be erosion by up to

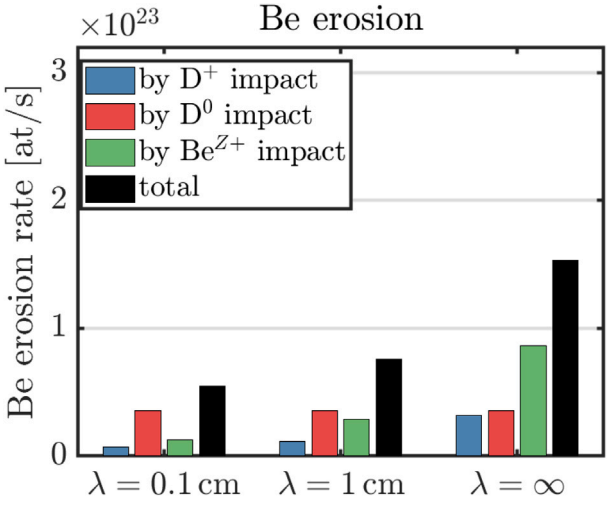

Fig. 3. Be erosion rate (integrated over the FW), obtained using different decay lengths. For each case, the contributions to erosion by different impacting species (D^+, D^0 and Be^{Z+}) are shown, as well as their sum.

a factor ~2. However, it must also be stressed that in the present approach, λ affects only the small extrapolation region shown in Fig. 2. Applying an exponential decay in the OEDGE extended grid region (pink shaded zone in Fig. 2), instead of the currently used flat curve fixed for consistency with the ITER HNLS assumptions, will lead to a more significant reduction of the predicted erosion.

2.3. Parameter scan B: Influence of particle impact angles

The Be sputtering yields used here are very sensitive to the impact angle, with a maximum yield at about $\theta \approx 80°$ and 70° for D and Be impact, respectively (with θ defined here relative to the surface normal, i.e. $\theta = 0$ corresponding to normal incidence) [5]. ERO2.0 requires assumptions on the impact velocity distributions of background D ions and neutrals to calculate the erosion, since these distributions are not contained in the input PBG. The following assumptions were used as default (reference case): (a) for D ions, the impact energy and angular distributions are obtained for each surface cell by following ion orbits in the magnetic pre-sheath and Debye sheath, with the approach (which was successfully benchmarked against PIC codes) described in more detail in [15]; (b) for D neutrals, the energy is set to the mean energy (provided by the PBGs) and the angle is set to the magnetic inclination angle θ_B. The plasma-wetted areas of the FW are associated with oblique magnetic inclination angles of $\theta_B > 80°$. Thus, with the above assumptions, neutrals have the same oblique impact angles $\theta = \theta_B$, whereas ions have distributions at about $\langle\theta\rangle \approx 70°$ and full width at half maximum (FWHM) $\approx 20°$ as shown in Fig. 4.

The assumption of $\theta = \theta_B$ for the neutrals in the reference case is a strong simplification, and could be considerably improved in the future by velocity distributions of CX deuterium obtained using a dedicated neutrals transport code such as EIRENE. For instance, an impact angle distribution closer to normal incidence is discussed in [16], which would result in lower sputtering yields. Thus, the current reference case assumption can be seen as an upper limit to the erosion by CX neutrals.

Moreover, the Be FW is assumed in the modelling as a perfectly smooth surface. In reality, the surface of FW components in ITER can be expected to exhibit a microscale roughness from manufacturing, which will, along with other factors, affect the impact angle distributions. The same is true for the castellation of the panels, which was neglected here. The effects of castellation and roughness on the impact of ions have been studied e.g. in [17–20]. However, the particle orbits before impact are affected by multiple parameters such as local magnetic field inclination, plasma parameters, and the size and form of the initial roughness, which is unknown for the ITER blanket and will likely change dynamically during plasma exposure. The in-detail investigation of these effects goes beyond the scope of this work. Nevertheless, as a first step it is important to investigate the dependence of the overall erosion on the impact angle, which is done here in a very general way by considering the entire possible range $\theta = 0$–90°.

In "parameter scan B", the particle impact assumptions are changed in the following way: for both ions and neutrals, the impact angle is set to a constant value θ_0 for all surface cells, regardless of the local geometry and plasma conditions. The value of θ_0 is subject to a parameter scan, with $\theta_0 = 0°, 40°, 60°, 75°, 80°$ and 85° for each simulation, respectively. Since the sheath tracing module was disabled in this scan, the ion energy distribution was simplified to the well-known analytic expression $E = 2T_i + q|V_{\text{sheath}}|$, where the first term is the thermal energy at the sheath entrance, and the second term is the energy gain due to the sheath acceleration [14, p. 629].

Fig. 5 shows the total, surface-integrated FW Be erosion plotted over the impact angle. In addition, the individual contributions of D^+, D^0 and Be^{Z+} impact are shown. The change in Be erosion due to D impact directly reflects the angular dependency of the sputtering yield curve, whereas the change in Be self-sputtering is a secondary effect due to the changing Be source strength. Due to an interplay of these two effects, the maximum of the total erosion is reached at about $\theta_0 = 80$–85°. The maximum value of $\Gamma^{\text{ero}}_{\text{Be}}(\theta_0 = 80°) = 2.35 \times 10^{23}$ Be/s is about 53 % higher than the reference case value of 1.53×10^{23} Be/s achieved with the broader impact angle distributions. On the other hand, the minimum value with $\Gamma^{\text{ero}}_{\text{Be}}(\theta_0 = 0°) = 1.28 \times 10^{22}$ Be/s is roughly 12x lower than the reference case value. One can estimate by linear interpolation that an erosion similar to the reference case can be achieved with a constant impact angle $\theta_0 \approx 70°$.

We can summarize that the reference case erosion of 1.53×10^{23} Be/s is in the upper middle part of the possible range 0.13–2.35×10^{23} Be/s that can be achieved by varying the impact angle between 0–90°. However, an assessment, validation or improvement of the impact angle distributions resulting from the reference assumptions would require knowledge of the surface roughness. In the case of the D neutrals, further insight could be gained in the future by using angular and energy distributions from EIRENE post-processing of the plasma backgrounds, combined with parameter studies using different types of roughness.

3. Parameter scan C: Influence of anomalous transport

ERO2.0 assumes a diffusion coefficient $D_\perp$ to account for anomalous cross-field transport of the Be test particles. The reference ERO2.0 case uses $D_\perp = 1\,\text{m}^2/\text{s}$, which is a typical empirically found value,[2] and is assumed here to be constant in the entire simulation domain. The choice of $D_\perp$ affects the transport of Be and its flux to the FW, and thereby the self-sputtering and net erosion/deposition fluxes. To investigate the importance of these effects, "parameter scan C" includes simulations with two different values for $D_\perp$ for Be transport: (1) a lower diffusion coefficient $D_\perp = 0.3\,\text{m}^2/\text{s}$ corresponding to the value used for D plasma transport in the SOLPS-4.3 simulations, and (2) a higher diffusion coefficient $D_\perp = 10\,\text{m}^2/\text{s}$.

Fig. 6 shows the total Be erosion for $D_\perp = 0.3\,\text{m}^2/\text{s}$ and $D_\perp = 10\,\text{m}^2/\text{s}$ along with the reference case $D_\perp = 1.0\,\text{m}^2/\text{s}$. For $D_\perp = 0.3\,\text{m}^2/\text{s}$, the total erosion is 28 % higher than in the reference case. For $D_\perp = 10\,\text{m}^2/\text{s}$ it is 37 % lower. Since $D_\perp$ affects only the Be transport in the ERO2.0 simulations, this change in erosion is entirely due to the self-sputtering contribution. As seen in Fig. 6 and Table 1, in the reference case Be self-impact contributes 56.2 % of the total erosion, while it is 65.8 % and 31.1 % in the $D_\perp = 0.3$ and $10.0\,\text{m}^2/\text{s}$ cases, respectively. As seen

[2] See [14], pp. 15, 158, 283.

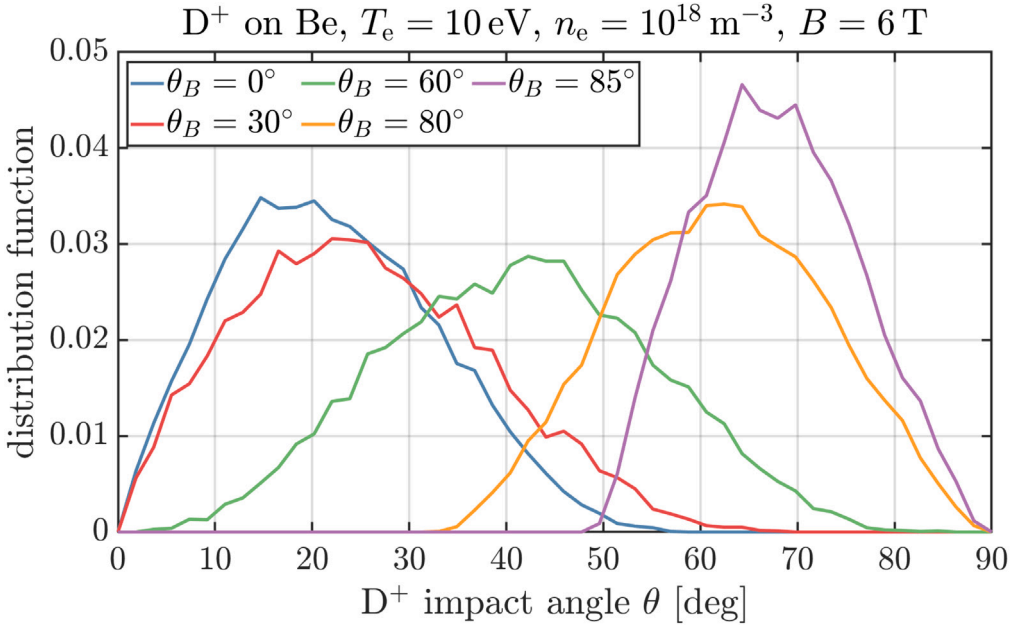

Fig. 4. Distributions of the impact angle θ for D^+ ions at different magnetic inclination angles θ_B, obtained using the sheath tracing module in ERO2.0.

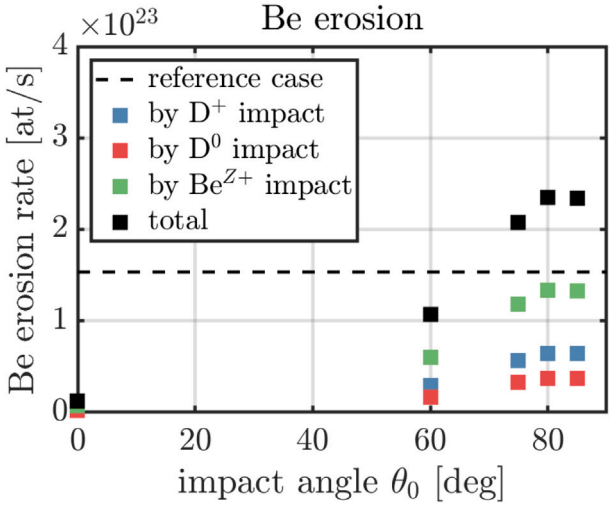

Fig. 5. Be erosion rate (integrated over the Be FW), obtained using different constant D^+ and D^0 impact angles θ_0.

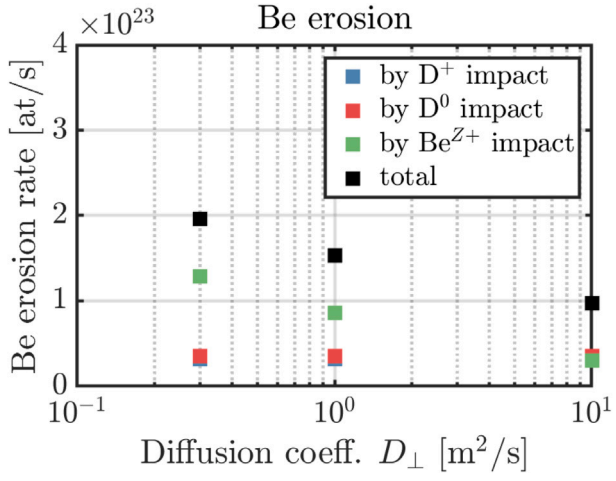

Fig. 6. Be erosion rate (integrated over the Be FW), obtained using different constant diffusion coefficients $D_\perp$.

in Table 1, increasing $D_\perp$ leads to a slightly increased Be redeposition flux on the FW (which can be explained by shorter migration paths due to higher probability of returning to the wall by cross-field transport). However, the changes in the Be charge and impact velocity distributions eventually lead to a decrease of the self-sputtering that far outweighs the increased flux.

To better understand the effect of the assumed $D_\perp$ on Be transport and self-sputtering, the distributions of Be impurities impacting on the FW are analysed. Fig. 7(a) shows the charge state distributions of impacting Be. One can see that a high diffusion coefficient $D_\perp = 10.0\,\mathrm{m^2/s}$ leads on the one hand to an increased fraction of singly charged Be, which is redeposited shortly after the erosion due to the radially outward diffusion, and on the other hand to an increased fraction of highly charged Be with Z = 3–4, which diffuses radially inward to the core plasma and eventually returns to the wall with a high energy. This is reflected in the Be impact energy distributions shown in Fig. 7(b), where $D_\perp = 10.0\,\mathrm{m^2/s}$ leads to an increase in both low-energy range ($E < 50\,\mathrm{eV}$) and high-energy tail ($E > 200\,\mathrm{eV}$), at the expense of the intermediate energy range (E = 50–200 eV). Finally, Fig. 7(c) shows the impact angle distributions. Increasing $D_\perp$ clearly leads to a shift towards lower Be impact angles associated with lower sputtering yields, thereby reducing the Be self-erosion. The most likely explanation for the shift to lower angles is that for higher $D_\perp$, Be penetrates more frequently into shadowed areas of the FW, which (due to the toroidal shaping of the panels) are characterized by less oblique magnetic incidence. This effect, together with the decreased fraction of particles in the intermediate energy range, outweighs the increase in erosion by the high-energy tail, leading to less self-erosion overall.

In summary, the variation of the perpendicular diffusion coefficient $D_\perp$ for Be ions over a wide range 0.3–10 $\mathrm{m^2/s}$ leads to a variation of the total erosion in the range $0.97–1.96 \times 10^{23}$ Be/s, due to the change in Be transport and Be self-sputtering. Importantly, the influence on the fractions of Be being deposited in the main chamber and divertor is negligible. The difference in self-sputtering is due to a change in the impact energy and angle distributions. As mentioned above, the studies

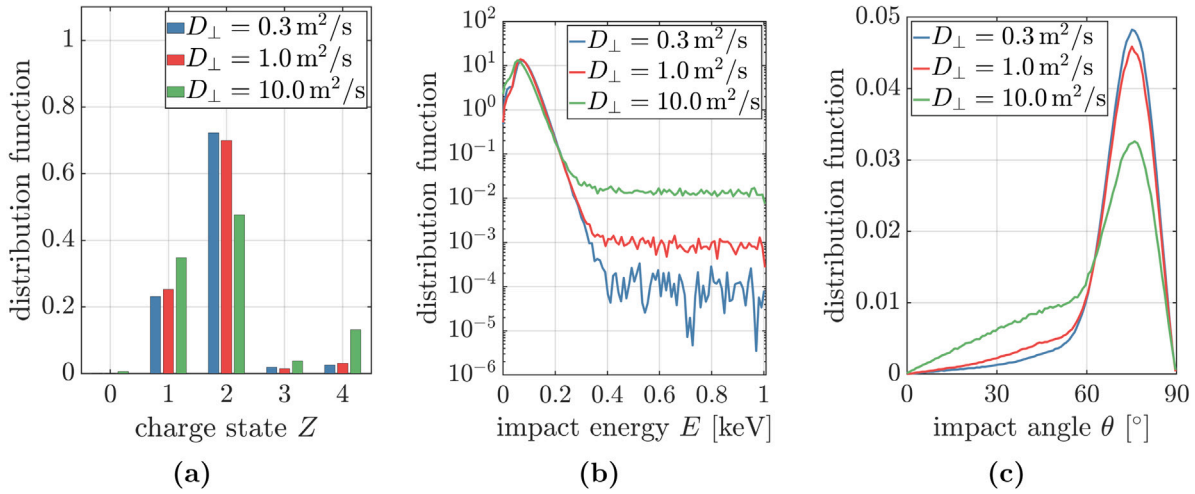

Fig. 7. Distributions of impacting Be, accumulated over the entire Be FW, for different values of $D_\perp$.

here are for perfectly smooth surfaces, and consideration of rough surfaces will likely affect the outcome for the angular distributions and thus self-sputtering.

4. Conclusions

Parameter studies have been performed to investigate the uncertainties on ERO2.0 modelling of beryllium erosion and migration in ITER under burning plasma conditions. The focus was on uncertainties related to plasma parameter extrapolation (scan A), impact velocity assumptions (scan B) and Be anomalous diffusion coefficient (scan C). The resulting variations of the total Be gross erosion were 0.55–1.53×10^{23} Be/s for scan A, 0.13–2.35×10^{23} Be/s for scan B, and 0.97–1.96×10^{23} Be/s for scan C. In scan A, the reference case with $\lambda = \infty$ and 1.53×10^{23} Be/s is the most conservative with the highest erosion, while in scans B and C, the reference case is found in the midrange of the possible values.

Judging from these numbers alone, the impact angle assumptions are the largest uncertainty (factor ~18 between minimum and maximum value), followed by the plasma extrapolation (factor ~3) and the diffusion coefficient (factor ~2). Although these error bars are very large, it must be noted that each of the scans was designed to cover a large range of values (or even the entire possible range, in the case of the impact angles). For instance, a decay length $\lambda = 0.1$ cm and an impact angle $\theta_0 = 0$ would both lead to an extreme reduction of the erosion. However, both assumptions holding simultaneously may be considered rather improbable. On the other hand, due to self-sputtering, the erosion depends in a non-linear way on the input parameters, which increases the overall uncertainty. Thus, a combination of moderate adjustments to input parameters could lead to a strong change of the total predicted erosion.

Further insight, and potentially a narrowing of the uncertainties, can be expected from the following actions:

- Arguably most important is the consideration of a representative surface roughness instead of a smooth surface, which would improve the impact angle distributions (and thus the erosion prediction) for all impinging particle species.
- Providing neutral impact energy and angular distributions from EIRENE would improve the predictions for erosion by CX neutrals impact.
- In general, ERO2.0 predictions are highly dependent on the input plasma backgrounds. In particular, further reducing the gap between grid boundary and FW surface in the input plasma background, e.g. by onion skin modelling or codes like EMC3-EIRENE and the upcoming version of SOLPS-ITER with an extended-grid functionality, would render the extrapolation of plasma parameters obsolete, thus improving the erosion prediction for ion impact.
- Castellation gaps were completely neglected in the present study. The majority of the erosion however is seen on enhanced heat flux (EHF) panels (e.g. 5, 8, 9), which have 12 mm square tile castellations. Field lines striking the sides of the castellations might have much closer to normal angles of incidence, which might reduce sputtering yields but at the same time increase the particle flux, which might increase total erosion. These effects should be investigated using a more precise wall geometry model that resolves the castellations.
- The input sputtering yield data for Be are another source of uncertainty, although the data used here have been validated experimentally at JET and PISCES-B [3]. However, the contribution of chemically assisted physical sputtering (CAPS) and subsequent transport of BeD molecules were neglected here for simplicity, and should be included in the future.

CRediT authorship contribution statement

J. Romazanov: Writing - original draft, Writing - review & editing, Software, Visualization, Conceptualization. **S. Brezinsek:** Writing - review & editing, Supervision, Resources, Project administration, Funding acquisition, Conceptualization. **R.A. Pitts:** Writing - review & editing, Supervision, Resources, Project administration, Funding acquisition, Conceptualization. **A. Kirschner:** Writing - review & editing, Supervision. **A. Eksaeva:** Writing - review & editing, Software. **D. Borodin:** Writing - review & editing, Software. **E. Veshchev:** Conceptualization. **V.S. Neverov:** Writing - review & editing, Software. **A.B. Kukushkin:** Conceptualization. **A.G. Alekseev:** Conceptualization. **Ch. Linsmeier:** Supervision.

Declaration of competing interest

The authors declare that they have no known competing financial interests or personal relationships that could have appeared to influence the work reported in this paper.

Acknowledgements

This work has been carried out within the framework of an ITER service contract with the ID IO/CT/18/4300001791. The views and opinions expressed herein do not necessarily reflect those of the ITER Organization.

The authors gratefully acknowledge the computing time granted by the JARA-HPC Vergabegremium on the supercomputer JURECA at Forschungszentrum Jülich.

References

[1] A. Huber, S. Brezinsek, V. Huber, M. Sertoli, G. Sergienko, I. Borodkina, M. Baruzzo, A. Kirschner, D. Borodin, J. Mailloux, S. Aleiferis, P. Carvalho, K. Lawsonf, Ch. Linsmeier, A. Meigs, S. Menmuir, Ph. Mertens, E. Pawelec, A. Shaw, JET Contributors, Erosion and Screening of Tungsten during inter/intra-ELM Periods in the JET-ILW Divertor, in: This Conference, 2021.

[2] A. Kirschner, D. Borodin, V. Philipps, U. Samm, R. Ding, K. Schmid, J. Roth, A. Kukushkin, G. Federici, A. Loarte, Estimations of erosion fluxes, material deposition and tritium retention in the divertor of ITER, J. Nucl. Mater. 390–391 (2009) 152–155, http://dx.doi.org/10.1016/j.jnucmat.2009.01.155.

[3] D. Borodin, J. Romazanov, R.A. Pitts, S.W. Lisgo, S. Brezinsek, I. Borodkina, A. Eksaeva, E. Safi, K. Nordlund, A. Kirschner, Ch. Linsmeier, Improved ERO modelling of beryllium erosion at ITER upper first wall panel using JET-ILW and PISCES-B experience, Nucl. Mater. Energy 19 (2019) 510–515, http://dx.doi.org/10.1016/J.NME.2019.03.016.

[4] J. Romazanov, S. Brezinsek, A. Kirschner, D. Borodin, A. Eksaeva, R.A. Pitts, S.W. Lisgo, H. Anand, E. Veshchev, V.S. Neverov, A.B. Kukushkin, A.G. Alekseev, Ch. Linsmeier, First Monte-Carlo modelling of global beryllium migration in ITER using ERO2.0, Contrib. Plasma Phys. 60 (5–6) (2019) e201900149, http://dx.doi.org/10.1002/ctpp.201900149.

[5] J. Romazanov, S. Brezinsek, A. Kirschner, A. Eksaeva, D. Borodin, R.A. Pitts, E. Veshchev, V.S. Neverov, A.B. Kukushkin, A.G. Alekseev, Ch. Linsmeier, Beryllium erosion and migration in different ITER plasma scenarios, Nucl. Fusion (2021) in preparation.

[6] D. Reiser, J. Romazanov, Ch. Linsmeier, On the possibility of track length based Monte-Carlo algorithms for stationary drift-diffusion systems with sources and sinks, J. Comput. Phys. 377 (2019) 219–231, http://dx.doi.org/10.1016/J.JCP.2018.07.051.

[7] R.A. Pitts, X. Bonnin, F. Escourbiac, H. Frerichs, J.P. Gunn, T. Hirai, A.S. Kukushkin, E. Kaveeva, M.A. Miller, D. Moulton, V. Rozhansky, I. Senichenkov, E. Sytova, O. Schmitz, P.C. Stangeby, G. De Temmerman, I. Veselova, S. Wiesen, Physics basis for the first ITER tungsten divertor, Nucl. Mater. Energy 20 (2019) 100696, http://dx.doi.org/10.1016/j.nme.2019.100696.

[8] S.W. Lisgo, A. Kukushkin, R.A. Pitts, D. Reiter, Design assessment of tungsten as an upper panel plasma facing material in ITER, J. Nucl. Mater. 438 (2013) S580–S584, http://dx.doi.org/10.1016/J.JNUCMAT.2013.01.121.

[9] D. Reiter, M. Baelmans, P. Börner, The EIRENE and B2-EIRENE codes, Fusion Sci. Technol. 47 (2) (2005) 172–186, http://dx.doi.org/10.13182/FST47-172.

[10] R.A. Pitts, S. Carpentier, F. Escourbiac, T. Hirai, V. Komarov, A.S. Kukushkin, S. Lisgo, A. Loarte, M. Merola, R. Mitteau, A.R. Raffray, M. Shimada, P.C. Stangeby, Physics basis and design of the ITER plasma-facing components, J. Nucl. Mater. 415 (1 SUPPL) (2011) S957—-S964, http://dx.doi.org/10.1016/j.jnucmat.2011.01.114.

[11] A.R. Raffray, B. Calcagno, P. Chappuis, Zhang Fu, A. Furmanek, Chen Jiming, D.H. Kim, S. Khomiakov, A. Labusov, A. Martin, M. Merola, R. Mitteau, S. Sadakov, M. Ulrickson, F. Zacchia, The ITER blanket system design challenge, Nucl. Fusion 54 (3) (2014) 18, http://dx.doi.org/10.1088/0029-5515/54/3/033004.

[12] Jülich Supercomputing Centre, JURECA: Modular supercomputer at Jülich Supercomputing Centre, J. Larg.-scale Res. Facil. 4 (A132) (2018) http://dx.doi.org/10.17815/jlsrf-4-121-1.

[13] S. Brezinsek, M.F.F Stamp, D. Nishijima, D. Borodin, S. Devaux, K. Krieger, S. Marsen, M. O'Mullane, C. Bjoerkas, A. Kirschner, JET EFDA Contributors, Study of physical and chemical assisted physical sputtering of beryllium in the JET ITER-like wall, Nucl. Fusion 54 (10) (2014) 103001, http://dx.doi.org/10.1088/0029-5515/54/10/103001.

[14] P.C. Stangeby, The Plasma Boundary of Magnetic Fusion Devices, IOP Publishing, Bristol and Philadelphia, 2000.

[15] I. Borodkina, D. Borodin, A. Kirschner, I.V. Tsvetkov, V.A. Kurnaev, M. Komm, R. Dejarnac, JET Contributors, An analytical expression for the electric field and particle tracing in modelling of be erosion experiments at the JET ITER-like wall, Contrib. Plasma Phys. 56 (6–8) (2016) 640–645, http://dx.doi.org/10.1002/ctpp.201610032.

[16] R. Behrisch, G. Federici, A. Kukushkin, D. Reiter, Material erosion at the vessel walls of future fusion devices, J. Nucl. Mater. 313–316 (SUPPL.) (2003) 388–392, http://dx.doi.org/10.1016/S0022-3115(02)01580-5.

[17] J.P. Gunn, S. Carpentier-Chouchana, F. Escourbiac, T. Hirai, S. Panayotis, R.A. Pitts, Y. Corre, R. Dejarnac, M. Firdaouss, M. Kočan, M. Komm, A. Kukushkin, P. Languille, M. Missirlian, W. Zhao, G. Zhong, Surface heat loads on the ITER divertor vertical targets, Nucl. Fusion 57 (4) (2017) 046025, http://dx.doi.org/10.1088/1741-4326/aa5e2a.

[18] K. Schmid, M. Mayer, C. Adelhelm, M. Balden, S. Lindig, Impact of gyro-motion and sheath acceleration on the flux distribution on rough surfaces, Nucl. Fusion 50 (10) (2010) 105004, http://dx.doi.org/10.1088/0029-5515/50/10/105004.

[19] Shuyu Dai, A. Kirschner, Jizhong Sun, D. Tskhakaya, Dezhen Wang, Modelling of surface roughness effects on impurity erosion and deposition in TEXTOR with a code package SURO/ERO/SDPIC, Nucl. Fusion 54 (12) (2014) 123015, http://dx.doi.org/10.1088/0029-5515/54/12/123015.

[20] A. Eksaeva, D. Borodin, J. Romazanov, A. Kirschner, A. Kreter, M. Eichler, M. Rasinski, A. Pospieszczyk, B. Unterberg, S. Brezinsek, C. Linsmeier, D. Tskhakaya, I. Borodkina, M. Komm, Surface roughness effect on Mo physical sputtering and re-deposition in the linear plasma device PSI-2 predicted by ERO2.0, Nucl. Mater. Energy 19 (2019) 13–18, http://dx.doi.org/10.1016/j.nme.2019.02.006.